International Journal of Hydrogen Energy 226 (2026) 154454

Contents lists available at ScienceDirect

International Journal of Hydrogen Energy

journal homepage: www.elsevier.com/locate/he

Kinetic origin of the sub-Nernstian cell voltage response in pressurised PEM water electrolysis

Katende Jonathan Kabamba [a], Tobias Binninger [b,*], Boris Bensmann [c], Rhiyaad Mohamed [a,**]

[a] HySA/Catalysis Centre of Competence, Catalysis Institute, Department of Chemical Engineering, University of Cape Town, 7701, South Africa
[b] Theory and Computation of Energy Materials (IET-3), Institute of Energy Technologies, Forschungszentrum Jülich GmbH, 52425, Jülich, Germany
[c] Leibniz University Hannover, Institute of Electric Power Systems, Appelstraße 9A, 30167, Hannover, Germany

ARTICLE INFO

Handling Editor: Søren Juhl Andreasen

Keywords:
PEM water electrolysis
Pressurised operation
sub-Nernstian voltage response
Electrochemical kinetics
Kinetic modelling

ABSTRACT

Proton-exchange-membrane water electrolysers (PEMWEs) can directly produce pressurised hydrogen, thereby reducing the need for downstream compression. Experimental studies have consistently reported a sub-Nernstian increase in PEMWE operating voltage under elevated pressure; however, existing modelling approaches have struggled to provide a satisfactory explanation for this behaviour. Here, a combined theoretical–experimental study is presented to elucidate the kinetic origin of pressure effects in PEMWE operation. Experiments conducted under differential and balanced pressurisation demonstrate a sub-Nernstian response of the PEMWE polarisation curve governed by cathode pressure, while anode pressurisation shows no kinetic effect. This behaviour is explained using a novel kinetic modelling framework that explicitly accounts for the distinct contributions of the oxygen evolution (OER), hydrogen evolution (HER), and hydrogen oxidation (HOR) reactions to the activation losses, formulated on a fixed reference potential scale. The model accurately reproduces the experimentally observed sub-Nernstian voltage response through simultaneous fitting of the polarisation data acquired at multiple operating pressures. In addition, the model provides a kinetic explanation for the deviations from linear Tafel behaviour observed at intermediate current densities.

1. Introduction

Hydrogen is a versatile energy carrier with multiple applications ranging from energy generation to feedstock for chemical industries [1–4]. It's use is expected to greatly contribute to the decarbonisation of industries where carbon emissions are hard to abate [5,6]. Hydrogen can be produced with very low carbon emissions by combining renewable energy sources and water electrolysis [7,8]; this can further address challenges associated with the intermittent nature of renewables like solar and wind via storage [9,10]. Among the different electrolysis technologies, proton exchange membrane water electrolysis (PEMWE) has emerged as one of the most promising, offering the advantage of high current density operation, high gas purity, compact design, high energy efficiency [7,11,12] and possibility of pressurised operation [13]. Pressurised PEMWE is gaining considerable interest, since hydrogen is often required at elevated pressures for storage, transportation [14] and other end uses [15,16]. Internal pressurisation of electrolysis gas has several advantages such as elimination of membrane dehydration resulting into the preservation of the integrity of the catalyst layer [17,18], reduced gas drying costs [17], and, most importantly, reduction of downstream gas compression costs [14,17,19,20]. High-pressure PEMWE experimental studies have been reported at pressures of 70 bar [21], 155 bar [22], 100 - 113 bar [4,14,23], and 180 bar [24], with the highest reported hydrogen output pressure of 700 bar [25]. Pressurised electrolysis operation can be carried out in either differential or balanced mode [17]. In differential mode, either the cathode (hydrogen) or anode (oxygen) gas is produced at an elevated pressure whilst the other is kept at atmospheric pressure. In balanced operation mode, gases are pressurised symmetrically in both anode and cathode compartments.

In standard modelling approaches, the total cell voltage is obtained by adding the various voltage losses (overvoltages) to the reversible voltage [21,26,27].

* Corresponding author.
** Corresponding author.
E-mail addresses: t.binninger@fz-juelich.de (T. Binninger), rhiyaad.mohamed@uct.ac.za (R. Mohamed).

https://doi.org/10.1016/j.ijhydene.2026.154454
Received 18 December 2025; Received in revised form 2 March 2026; Accepted 8 March 2026
Available online 18 March 2026
0360-3199/© 2026 The Authors. Published by Elsevier Ltd on behalf of Hydrogen Energy Publications LLC. This is an open access article under the CC BY license (http://creativecommons.org/licenses/by/4.0/).

$$V = V_{eq} + \eta_{act} + \eta_{ohm} + \eta_{mt} \quad (1)$$

Where the reversible voltage (V_{eq}) is the minimum theoretical cell voltage required to split water into oxygen and hydrogen, the activation overpotential (η_{act}) arises from the activation energy required to overcome the activation barriers of the electrode reactions, the ohmic overvoltage (η_{ohm}) is due to resistance to the flow of protons and electrons across cell components and interfaces, and the mass transport overpotential (η_{mt}) arises from mass-transport limitations of reactants and products to and from the active sites of the catalyst [7,28]. Elevating the operation pressure is expected to require an increased energy input in the form of an increased cell voltage. The effect of pressure on the reversible (or equilibrium) cell voltage (V_{eq}) is described by the Nernst equation:

$$V_{eq} = V_0 + \frac{RT}{4F} \ln\left(\frac{P_{O_2}}{P_0}\right) + \frac{RT}{2F} \ln\left(\frac{P_{H_2}}{P_0}\right) \quad (2)$$

where P_{O_2} and P_{H_2} are the oxygen and hydrogen pressures at the anode and cathode, respectively, T is the operating temperature, R the gas constant, and F the Faraday constant. The standard equilibrium voltage, V_0, corresponds to the equilibrium cell voltage under standard pressure, $P_0 = 1$ bar. The Nernstian increase of the cell voltage according to Eq. (2), multiplied with the number of electrons exchanged per gas molecule ($2e^-$ per H_2 and $4e^-$ per O_2), corresponds to an (increased) electrical energy input that is precisely equal to the energy of isothermal compression of the product gases from P_0 to P_{O_2} and P_{H_2}. Therefore, as required by thermodynamics, the minimum energy need for pressurised electrolysis at the target pressures of P_{O_2} and P_{H_2} is the same as for electrolysis performed at P_0 followed by post-electrolysis compression to P_{O_2} and P_{H_2}.

In practice, the Nernstian voltage increase of Eq. (2) is considered the basic contribution of pressure to the PEMWE operation voltage, onto which irreversible contributions of activation losses, ohmic losses, and mass-transport losses are added [29–32]. At the simplest level, the activation overvoltage as a function of cell current density (i) is described by the Tafel equation: $\eta_{act} = (RT/\alpha F) \ln(i/i_0)$, with transfer coefficient α and exchange current density i_0. The ohmic overvoltage is given by $\eta_{ohm} = iR_{ohm}$ with the overall cell resistance R_{ohm}. No simple expression is generally given for the mass-transport overvoltage. Based on this voltage decomposition, the "trivial" Nernstian shift of the reversible voltage (Eq. (1)), a function of P_{H_2} and P_{O_2}, appears to define a lower bound for the increase in cell voltage with increasing operating pressures while the effect of pressure on the overvoltages is less obvious. Accordingly, experimentally observed sub-Nernstian voltage increases have often been attributed to pressure-induced changes in reaction kinetics [33], although their underlying origin has remained unclear. In this work, a different modelling approach with a focus on pressure effect on reaction kinetics is pursued, which, as will be seen, provides a comprehensible explanation for the sub-Nernstian response of the cell voltage.

Experimental studies confirmed the increase of PEMWE cell voltage at elevated cathode pressures in differential mode [14,34–36]. The findings were attributed to: (i) an increase in the reversible cell voltage with increasing pressure according to the Nernst shift [14,32], (ii) an increase in reversible cell voltage and mass transport losses [31], or (iii) an increase in the reversible cell voltage and ohmic losses at higher pressures [22]. However, several studies also reported "beneficial" effects of increased pressure on PEMWE performance [14,18,37–40], meaning that the operation cell voltage increased less than predicted by the Nernst equation, or even decreased at elevated operation pressure. Grigoriev et al. [18] were the first to report an improvement in cell performance at elevated pressures. Suermann et al. [14] observed that the pressure effects on cell voltage were minor at current densities above 1 A/cm^2 in balanced pressure mode. In the same study, the expected isothermal compression behaviour was reported in differential operation mode at ambient anode pressure. In another study conducted in differential mode (constant anode pressure), at current densities above 0.3 A/cm^2, and higher cathode pressures, cell voltage shifts increasingly lower than expected from isothermal compression behaviour were reported [39]. A similar observation was made by Bernt et al. [40] for studies conducted in balanced pressure mode. In the same studies, the cell voltage at 30 bar was reported to be lower than at 1 bar for current densities above 4.5 A/cm^2. The improvements in performance were often entirely attributed to a decrease in mass transport losses at higher pressures; this resulted from smaller gas bubbles formed leading to reduced catalyst surface blocking [38,40].

When analysing the different contributions to the total cell voltage, most studies have considered pressure as a factor primarily affecting the reversible cell voltage and mass transport losses. Studies on the effects of pressure on kinetic losses are scarce and come to inconsistent conclusions. Some authors have reported an increase in activation losses with increasing pressure in differential operation mode at constant anode pressure [21,35], whereas others observed a decrease in kinetic losses in balanced pressure mode with increasing pressures due to possible increase of catalyst effective electrochemical surface are [33] or better electrodes compression and local temperature increase [4] at higher pressures. Suermann et al. [14] suggested that both kinetic and mass transport losses decrease at higher pressures resulting in the overall cell performance improvement observed in balanced operation mode. The Tafel model was used to explain the improvements in reaction kinetics. It was suggested that higher pressures lead to increased specific exchange current density due to changes in the standard Gibbs free energy of activation of the rate determining step. In another study, the authors concluded that pressure did not affect PEMWE reaction kinetics of the OER and HER occurring in the liquid phase, and only thermodynamic and mass transport components of the cell voltage were affected [41]. The differing results and interpretations presented in the literature highlight the need to better understand how electrolyser performance and electrolysis kinetics are affected by both differential and balanced pressurisation of cathode and anode compartments.

Recent theoretical arguments have supported the kinetic origin of a sub-Nernstian response of cell voltage to pressure increase [42]. It was put forth that the thermodynamic Nernstian shift of the reversible voltage results from the shift in the dynamic equilibrium between forward and reverse directions of the electrode reactions, *i.e.*, the hydrogen evolution reaction (HER) and hydrogen oxidation reaction (HOR) for the hydrogen electrode and the oxygen evolution reaction (OER) and oxygen reduction reaction (ORR) for the oxygen electrode. Since hydrogen and oxygen are the reactants for the HOR and ORR, respectively, their respective pressures primarily affect the rates of the HOR and ORR, which, under electrolysis operation conditions, have a minor to negligible effect on the overall net reaction rate of the water electrolysis reaction.

In the present work, the influence of operation pressure on reaction kinetics in PEMWE is studied by a combined theoretical–experimental approach. Previous studies on PEMWE performance and modelling have almost exclusively used the Nernst equilibrium voltage of the system under given operation conditions, i.e., pressures, as reference to define kinetic overvoltage and overpotentials. In this conventional approach, the treatments of equilibrium and reaction kinetics are clearly separated. In this study, a new model for the current–voltage relationship in pressurised PEMWE is presented. As a main difference to previous approaches, the kinetic overpotentials of both electrode reactions are defined relative to a respective fixed reference potential. With this approach, the intertwined nature of equilibrium and kinetics is emphasized, which is based on the principle of a dynamic equilibrium in terms of a balance between the forward and backward reaction kinetics. The Nernst shifts of equilibrium potentials and reversible cell voltage with pressure changes are thus implicitly included in the kinetic equations for the hydrogen and oxygen electrode reactions, explicitly accounting for the pressure dependencies via respective reaction orders. It

is shown that this change in perspective from the common shifting equilibrium to a fixed potential reference in electrode kinetics readily explains the experimentally observed pressure dependence of the PEMWE voltage at low to moderate current densities.

2. Model development

2.1. Cell voltage equation

As a main difference to the typical model for the cell voltage of Equation (1), the model developed here takes the fixed equilibrium voltage (V_0) under standard pressure as a reference, and not the (pressure-dependent) shifting equilibrium voltage (V_{eq}, cf. Equation (2). The model equation for the total cell voltage reads

$$V = V_0 + \left(E_a - E_{a,0}\right) - \left(E_c - E_{c,0}\right) + \eta_{ohm} + \eta_{mt} \tag{3}$$

where V_0 is the reversible voltage at operation temperature (T) under standard hydrogen and oxygen pressures of 1 bar, which is described by the empirical expression [43]

$$V_0 = 1.229\ \mathrm{V} - 8.46 \times 10^{-4}\ (\mathrm{V/K})(T - 298\ \mathrm{K}) \tag{4}$$

$E_a - E_{a,0}$ and $E_c - E_{c,0}$ are the kinetic overpotentials of the anode and cathode electrodes, respectively, where $E_{a,0}$ and $E_{c,0}$ are the corresponding fixed equilibrium potentials under standard pressures, with $V_0 = E_{a,0} - E_{c,0}$. The kinetic overpotentials are determined by the kinetic models described in the next section. The use of the fixed potential/voltage reference is the main difference to standard modelling approaches and key to the explanation of experimentally observed sub-Nernstian effects. It will be shown that the present approach is fully consistent with the Nernstian shift of the *equilibrium* potentials/voltage for given pressures in Section 2.3.

The focus of this work is the unified treatment of the interrelated pressure dependencies of equilibrium and kinetic terms. Ohmic losses are treated as usual by the ohmic overvoltage $\eta_{ohm} = iR_{ohm}$, caused by the overall ohmic resistance of the cell. This term is subtracted from the measured polarisation curves before data fitting, using the value of the high frequency resistance (HFR) obtained from impedance measurements, cf. section 3.2.

2.2. Kinetic model for electrode reactions

The overall water splitting reaction is the sum of the anodic and cathodic half-cell reactions,

$$\textbf{\textit{Anode reaction}} \quad 2H_2O \rightleftarrows O_2 + 4H^+ + 4e^- \tag{5}$$

$$\textbf{\textit{Cathode reaction}} \quad 4H^+ + 4e^- \rightleftarrows 2H_2 \tag{6}$$

$$\textbf{\textit{Overall reaction}} \quad 2H_2O \rightleftarrows 2H_2 + O_2 \tag{7}$$

In the present modelling approach, the electrode reactions are treated separately. Moreover, for each of the half-cell reactions, both the forward and backward directions are explicitly considered, *i.e.*, the oxygen evolution reaction (OER) and oxygen reduction reaction (ORR) at the PEMWE anode (left-to-right and right-to-left in (5), respectively) and the hydrogen evolution reaction (HER) and hydrogen oxidation reaction (HOR) at the PEMWE cathode (left-to-right and right-to-left in (6), respectively).The net kinetic current of the hydrogen electrode reaction (6) is modelled by a generalised Butler-Volmer equation [44], where the kinetic overpotential $E_c - E_{c,0}$ is quantified with respect to the *fixed* equilibrium potential $E_{c,0}$ under standard hydrogen pressure of $P_0 = 1$bar,

$$i_{kin,c} = i_{0,c}\left(\left(\frac{P_{H_2}}{P_0}\right)^{m_{HOR}} e^{\left(\frac{\alpha_{HOR}F}{RT}\left(E_c - E_{c,0}\right)\right)} - \left(\frac{P_{H_2}}{P_0}\right)^{m_{HER}} e^{-\left(\frac{\alpha_{HER}F}{RT}\left(E_c - E_{c,0}\right)\right)}\right) \tag{8}$$

The first and second terms describe the (competing) rates of the backward (HOR) and forward (HER) reactions, respectively, with charge transfer coefficients α_{HOR} and α_{HER}, reaction orders m_{HOR} and m_{HER} in H_2 pressure dependence, and exchange current (density) $i_{0,c}$ at the reference potential $E_{c,0}$. The hydrogen-pressure effect is explicitly accounted for in terms of the reaction orders m_{HOR} and m_{HER}. The generalised Butler-Volmer equation (8) is an approximate form of the rate equations from microkinetic models for the HER/HOR [45,46], obtained under the assumption of a constant coverage of the catalyst surface with the reaction intermediate [44]. It is highlighted that in the present modelling approach, the rate expression is formulated on a fixed potential scale, using the equilibrium potential $E_{c,0}$ under standard hydrogen pressure of $P_0 = 1$bar as a reference. This is opposed to the commonly used overpotential scale that shifts with the equilibrium potential for given operation pressures.

It must be emphasized that the present study does not aim to draw any conclusions regarding the microkinetic mechanism of the HER/HOR under PEMWE conditions. Due to the fast kinetics under acidic conditions, detailed mechanistic studies are challenging, and no final conclusion on this question has been reached yet [46–50]. The Heyrovsky–Volmer or Tafel–Volmer mechanisms with different possible rate-determining steps are commonly considered, imposing different conditions on the values of transfer coefficients and reaction orders. Readers interested in detailed explanations on conditions for HER/HOR kinetic parameters imposed by microkinetics are directed to the extensive discussion in Section S.1 of the supporting information (SI), as well as in a recent study on the HER/HOR kinetics under alkaline conditions [44]. Since a detailed mechanistic discussion lies outside the scope of the present study, it was decided to focus on the model with $\alpha_{HOR} + \alpha_{HER} = 1$ and fixed reaction orders of $m_{HOR} = 1/2$ and $m_{HER} = 0$ in the following, which provided the best consistency of the fitted parameter values between the different pressurisation modes, *cf.* Table 1. Fitted parameters corresponding to an alternative flavour of the model with $\alpha_{HOR} + \alpha_{HER} = 2$ and fixed reaction orders of $m_{HOR} = 1$ and $m_{HER} = 0$, is shown in Table S.1 in the SI, with corresponding plots of experimental and fitted polarisation curves shown in Fig S.1 and Fig S.2. It is again emphasized that the choice of these parameter combinations is not unique, and the present study does not aim to draw any definite conclusions on the HER/HOR reaction mechanism under PEMWE conditions. Importantly, the main findings and conclusions of this work do not depend on the kinetic model flavour used for data fitting. Moreover, we have included the results for alternative model flavours in the SI to demonstrate the robust nature of the study's main findings. It should be

Table 1
Values of the electrochemical model parameters (with $\alpha_{HOR} + \alpha_{HER} = 1$ and fixed reaction orders of $m_{HOR} = 1/2$ and $m_{HER} = 0$) fitted to the experimental data sets of three different PEMWE pressurisation modes: cathode differential, anode differential, and balanced pressurisation. Also given is the standard deviation of each fitting parameter and the root mean square deviation (RMSD) between experimental data and model fits.

Parameters	Cathode pressurisation	Anode pressurisation	Balanced pressurisation
$i_{0,a}$ [A/cm^2]	$(5.03 \pm 0.30) \times 10^{-8}$	$(1.84 \pm 0.35) \times 10^{-7}$	$(8.28 \pm 0.58) \times 10^{-8}$
$i_{0,c}$ [A/cm^2]	1.08 ± 0.01	0.82 ± 0.05	1.38 ± 0.03
α_{OER}	1.48 ± 0.01	1.34 ± 0.02	1.42 ± 0.01
α_{HER}	0.27 ± 0.01	0.40 ± 0.02	0.31 ± 0.01
$\alpha_{HOR} = 1 - \alpha_{HER}$	0.73 ± 0.01	0.60 ± 0.02	0.69 ± 0.01
RMSD [V]	0.0015	0.0134	0.0016

emphasized that structure and key components of the kinetic model are the same across all model flavours, which only differ in the numeric values of certain parameters (and parameter combinations). The fact that macroscopic conclusions hold true irrespective of "model flavour" indicates that agreement is not due to overfitting, but that the basic structure and setup of the kinetic model equations grasp the essential physics (and chemistry) underlying the macroscopically observable effects.

Similar to Eq. (8), the net kinetic current of the oxygen electrode reaction (5) is modelled by a Butler-Volmer-type expression of the form

$$i_{\mathrm{kin,a}} = i_{0,\mathrm{a}} \left(e^{\left(\frac{\alpha_{\mathrm{OER}} F}{RT} \left(E_{\mathrm{a}} - E_{\mathrm{a},0} \right) \right)} - \left(\frac{P_{\mathrm{O_2}}}{P_0} \right) e^{-\left(\frac{\alpha_{\mathrm{ORR}} F}{RT} \left(E_{\mathrm{a}} - E_{\mathrm{a},0} \right) \right)} \right) \tag{9}$$

where α_{OER} and α_{ORR} are the charge transfer coefficients of the forward (OER) and backward (ORR) reactions, respectively, and $i_{0,\mathrm{a}}$ is the exchange current (density) at the fixed reference potential $E_{\mathrm{a},0}$ under standard oxygen pressure of $P_0 = 1\mathrm{bar}$. Under PEMWE conditions, the ORR rate (second term in brackets) is negligible, but it is still formally included in the rate expression (9) to make the overall model consistent with the Nernst equation as discussed below. As for the hydrogen electrode reaction, the Butler-Volmer model (9) represents a semi-empirical simplification of the more complicated rate equations obtained from microkinetic models for the OER/ORR. With oxygen being the reactant for the ORR backward reaction (cf. Eq. (5)), the oxygen pressure is assumed to only influence the ORR rate (second term in brackets), leaving the OER rate (first term in brackets) unaffected, as supported by results from rotating disk electrode experiments [51]. This observation is explained by the basic principle that electrochemical multi-step kinetics typically approach single-step behaviour at large overpotentials, as is the case for the OER. In this regime, the rate-determining step gets typically shifted to the reactant side, making the (forward) rate independent of the concentration of products.

Under PEMWE operation, the cell current, i, is generated by the cathode and anode electrode reactions, thus requiring

$$i = -i_{\mathrm{kin,c}} = i_{\mathrm{kin,a}} \tag{10}$$

This condition, together with Eqs. (8) and (9), determines the cathode and anode overpotentials, $E_{\mathrm{c}} - E_{\mathrm{c},0}$ and $E_{\mathrm{a}} - E_{\mathrm{a},0}$, as a function of the cell current. Since Eqs. (8) and (9) cannot be resolved analytically, a numerical algorithm is required (cf. section S.2 in SI).

2.3. Nernst condition

The conventional voltage model of Eq. (1) employs the reversible (equilibrium) voltage V_{eq} as a reference that shifts with changes in hydrogen and oxygen pressures according to the Nernst equation (2). In contrast, the present model of Eq. (3) uses V_0 as a fixed reference that is not affected by changes in operation pressures. Such an approach implies that the thermodynamically required Nernstian shift of the equilibrium voltage is captured by the kinetic terms, $E_{\mathrm{a}} - E_{\mathrm{a},0}$ and $E_{\mathrm{c}} - E_{\mathrm{c},0}$, as shown in the following. At equilibrium, $E_{\mathrm{a}} = E_{\mathrm{a,eq}}$ and $E_{\mathrm{c}} = E_{\mathrm{c,eq}}$, no current is flowing through the cell, $i = 0 = i_{\mathrm{kin,c}} = i_{\mathrm{kin,a}}$. Setting the left-hand sides of Eqs. (8) and (9) to zero and resolving for the respective potentials yields:

$$E_{\mathrm{a,eq}} - E_{\mathrm{a},0} = \frac{RT}{(\alpha_{\mathrm{OER}} + \alpha_{\mathrm{ORR}})F} \ln\left(\frac{P_{\mathrm{O_2}}}{P_0} \right) \tag{11}$$

$$E_{\mathrm{c,eq}} - E_{\mathrm{c},0} = -\frac{RT}{(\alpha_{\mathrm{HOR}} + \alpha_{\mathrm{HER}})F} \ln\left(\frac{P_{\mathrm{H_2}}}{P_0} \right)^{m_{\mathrm{HOR}} - m_{\mathrm{HER}}} \tag{12}$$

Inserted into Eq. (3), this gives the cell voltage at equilibrium,

$$V_{\mathrm{eq}} = V_0 + \frac{RT}{(\alpha_{\mathrm{OER}} + \alpha_{\mathrm{ORR}})F} \ln\left(\frac{P_{\mathrm{O_2}}}{P_0} \right) + \frac{RT}{(\alpha_{\mathrm{HOR}} + \alpha_{\mathrm{HER}})F} \ln\left(\frac{P_{\mathrm{H_2}}}{P_0} \right)^{m_{\mathrm{HOR}} - m_{\mathrm{HER}}} \tag{13}$$

which is consistent with the Nernst equation (2) provided that $\alpha_{\mathrm{OER}} + \alpha_{\mathrm{ORR}} = 4$ and $\alpha_{\mathrm{HOR}} + \alpha_{\mathrm{HER}} = 2(m_{\mathrm{HOR}} - m_{\mathrm{HER}})$. These requirements, imposed in data fitting, are set to ensure consistency between kinetic formulation and principles dictated by thermodynamics. The Nernst equation is obtained at net current of 0 for adequate formulation of electrode kinetics [52]. Moreover, without constraints, the larger number of free model parameters would make the fitting results ambiguous.

2.4. Model assumptions and justification

Mass-transport losses are assumed to be negligible within our experimental current density range (and for the cell setup employed). Our primary argument to justify this assumption is the simple fact that the basic version of our model, which does not include any mass transport terms, is able to accurately describe the experimental data across the entire current density range studied (and at multiple operating conditions), as shown in the Results and Discussion sections. An additional mass transport term would be redundant and lead to overfitting. In other words, no mass transport terms are required to explain our experimental observations, and our basic kinetic model accounting for fundamental rules of chemical reaction kinetics is sufficient.

In the present literature, the onset of transport limitations is highly debated; theoretical models have suggested contributions of mass transport even at low current densities (<100 mA/cm^2) [53]. Suermann et al. [33] have reported transport losses at currents > 200 mA/cm^2 using their own in-house electrolyser cell design [53]. In modelling studies conducted in Refs. [29,54–58] mass transport limitations were assumed to be negligible. It is reported that the nominal operating current density of state-of-the-art PEMWE, determined by the manufacturer, is not high enough for mass transport limitations to occur [27,59]. In the case of Giner electrolysers operated between 3 and 5 A/cm^2, there has been no evidence of mass transport limitations [60]. Moreover, for the cell configuration used in the present study, recent investigations support the negligible mass transport assumption. The study suggested that mass transport limitations are not relevant in PEMWE up to 25 A/cm^2 [61]. Furthermore, transport losses have been reported to be negligible at water stoichiometries above 5 [62], a value significantly exceeded in our study. Refs [40,63] reported no limiting current behaviour and suggested insignificant mass transport contributions due to PTL pore dry-out associated with gas displacement of liquid water at high current densities. They recommended avoiding categorisation of "residual overpotential" as "mass transport" unless the presence of pore-phase fluid limitation can be demonstrated. The negligible mass transport assumption for the maximum selected current density (1.2 A/cm^2) in our study is therefore well supported by literature.

Previous studies reported hydrogen oxidation reaction (HOR) currents due to permeated H_2 consumption in differential pressure mode [64,65]. Ref. [65] highlighted high conversion of permeated H_2 at low current densities and applied current density corrections to account for this effect. In contrast, our study assumes negligible hydrogen crossover effects on cell voltage. This is justified by the observation in our results that at low current densities, the voltage response to cathode pressure increase (under ambient anode pressure) strictly follows the thermodynamic Nernstian shift.

In the present work, the kinetic overpotential is described using a generalised Butler-Volmer framework. While detailed microkinetic modelling offers insight into elementary reaction steps, it lies outside the scope of this study, which focuses on macroscopic kinetic trends rather than fundamental mechanistic determination. Furthermore, the model is restricted to the low to mid current density region where mass transport

losses are assumed negligible; this allows for the isolation of kinetic effects.

2.5. Model validation and data fitting

The mathematical model described above was implemented using the open-source software Python. Information on model validation technique and data fitting is shown in S.2 of SI. The integrated procedure of modelling and experiment is summarised in Fig. 1 involving model development based on the PEMWE operating parameters, model implementation in Python, experimental data acquisition, and data fitting and model validation.

Before executing the fitting routine, the reaction orders were fixed ($m_{HOR} = 1/2$ and $m_{HER} = 0$) for reasons described in section 2.2. while $i_{0,a}$, $i_{0,c}$, α_{OER}, and α_{HER} were designated as free parameters to be fitted to the experimental polarisation curves. The partial pressures of H_2 at the cathode and O_2 at the anode as they appear in the model equations (Eqs (8 and (9) were fixed to the values of the controlled pressures of their respective compartments, thereby neglecting the possible influence of water vapor. At the operating temperature of 60 °C, the water vapor saturation pressure of 0.199 bar introduces a negligible deviation to the calculated Nernstian shifts. This assumption is considered robust for the present data analysis as the deviation falls within the margins of experimental uncertainty.

3. Experimental procedure

3.1. Materials and setup

Commercial catalyst coated membranes (CCMs) from HIAT were

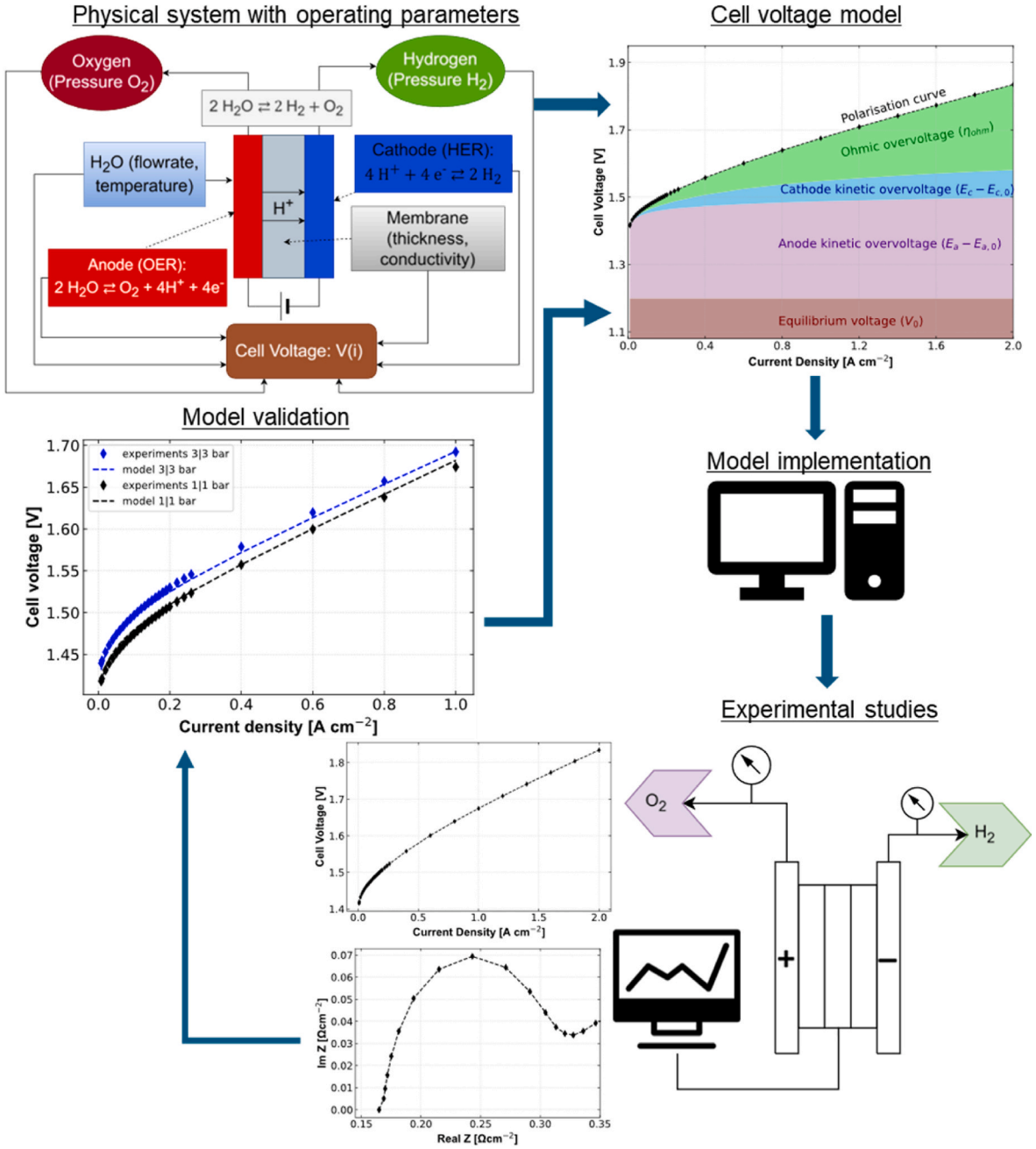


Fig. 1. Schematic illustrating the process of electrochemical model development, implementation, and validation by fitting to experimental PEMWE polarisation data under different operation pressures.

used for this study. They are made of a Nafion 115 membrane coated on the anode side with 2 mg_{Ir}/cm^2 iridium black-based catalyst and on the cathode side with 1 mg_{Pt}/cm^2 carbon-supported platinum catalyst. Sintered titanium fibres 1 mm thick with a fibre diameter of 0.20 mm (2GDL40 – 1.00, Bekaert) were used as porous transport layers (PTLs) on the anode side and carbon PTLs (E20H, Freudenberg SE) with hydrophobic treatment were used for the cathode side.

A 4 cm^2 electrolyser cell from Fraunhofer ISE was used for measurements. It is made of gold coated titanium current collectors and end plates equipped with flow fields. The frame where the cell is mounted comprises a screw perpendicular to the base of the cell which is adjusted to apply the desired clamping force. A load cell located between the screw and the cell is used to monitor the clamping force. The electrochemical measurements were carried out in a E100 test bench from Greenlight Innovation connected to an SP-150 BioLogic potentiostat with a 20 A Booster. The test bench was equipped with a pressure booster for rapid increase of hydrogen and oxygen gas pressures to the desired values.

3.2. Measurement protocol

The cell was mounted onto the test bench after assembly. The feedwater, flowing at 100 ml min^{-1}, was used to heat up the cell to the desired temperature (60 °C in this study) and circulated for 1 h for thermal conditioning of the cell. A 3 kN clamping force was applied on the cell after thermal conditioning. Subsequently, galvanostatic conditioning steps at 0.2, 1, and 1.4 A/cm^2 were carried out for 30 min each. The cell was then conditioned at a constant voltage of 1.7 V for 1 h prior to measurements. Since the focus of this study lies on exploring the intertwined thermodynamic and kinetic pressure effects, a current density range up to 1.2 A/cm^2 with minimum mass transport limitations [66] was selected. In this range, only kinetic and ohmic losses are expected to be significant, which is confirmed by the very good agreement of our fitted model with the experimental data as shown and discussed in the Results and Discussion. Polarisation curves were measured in 0.01 A/cm^2 steps up to 0.1 A/cm^2, then in 0.1 A/cm^2 steps up to 1.2 A/cm^2. It should be mentioned that PEMWE operation currents typically exceed the range studied here. Other phenomena related to mass transport and bubble formation, which can become relevant at higher current densities, lie outside the scope of this work. However, it is emphasized that the kinetic effect remains a relevant contribution also at high current densities. The basic understanding of the intertwined thermodynamic–kinetic pressure effect provided by the present study will therefore be foundational for disentangling the more complex pressure effects at larger current densities in future studies.

The present approach facilitates the deconvolution of voltage losses for studying the kinetic pressure effect. Moreover, the relatively low upper limit of the current density range ensured that irreversible changes and degradation were minimised to guarantee maximum comparability of polarisation curves subsequently recorded at different pressures. Electrochemical impedance spectroscopy (EIS) measurements were conducted for each current density step at frequencies ranging from 100 kHz to 100 Hz with 6 points per decade, and the high frequency resistance (HFR) was obtained from the real axis intercepts of the respective Nyquist plots. The polarisation curve measurements were performed twice in both ascending and descending directions, and the average of the 4 curves, or data points, at each current density was used for further analysis. In this work, current densities are defined with respect to the geometric area of the cell (and not the catalyst surface area), as in-situ ECSA quantification for Iridium-based catalysts used at the anode remain challenging [67]. However, since identical catalyst loadings were used for all tests, geometric normalisation provides a consistent basis for the quantitative and qualitative comparison of pressure induced effects reported here.

Measurements were conducted at operation pressures ranging from 1 to 10 bar in both differential and balanced pressure modes. This moderate pressure regime was targeted for two reasons: first, to maintain relevance to typical commercial PEMWE units which are designed for a maximum hydrogen pressure of 30 – 40 bar [24]; second, and most important, to focus on the investigation of the pressure effect on reaction kinetics, minimising unwanted side effects, whilst still producing sufficiently large variations in the data for meaningful analysis with minimum statistical error margins. In between measurements, during change of the pressure to the next set value, a current density of 1 A/cm^2 was applied and the pressure boost function of the test station was activated. For each pressure mode (differential, balanced), measurements were conducted in descending order, *i.e.*, from 10 to 1 bar on the same cell. After the measurement at 1 bar, a final polarisation curve was recorded at the starting pressure of 10 bar to assess the occurrence of irreversible changes during the experiment. In all cases, the initial and final polarisation curves agreed to within 2 mV maximum, demonstrating excellent reliability of the data.

4. Results

Investigations were conducted on the effect of pressure on cell polarisation behaviour for differential and balanced modes. In differential mode, both the effect of cathode pressure at ambient (1 bar) anode pressure and the effect of anode pressure at ambient cathode pressure were studied. Measured and iR-free polarisation curves together with fitted model curves for different operating pressures are shown in Fig. 2 for differential modes and Fig. 4 for balanced mode. The corresponding fitted model parameters are compiled in Table 1 and further analysed in the Discussion section. As explained in Section 2.2, the results shown here correspond to the kinetic model with $\alpha_{HOR} + \alpha_{HER} = 1$ and fixed reaction orders of $m_{HOR} = 1/2$ and $m_{HER} = 0$. In the SI, we report the covariance matrices of the fitted parameters (Table S.2). These provide a basis for the discussion on the sensitivity of cell voltage to fitting parameters.

Differential mode: cathode pressurisation. Fig. 2a shows the total and iR-free cell voltage as a function of current density under different cathode pressures and a constant anode pressure of 1 bar. An overall increase in cell voltage with cathode gas pressure is observed. After iR-correction, the iR-free cell voltage increases with cathode gas pressure following a trend similar to the total cell voltage. This shows that the changes in HFR with cathode gas pressure are negligible. Fig. 3 shows these changes to fall within the experimental error. The net difference between the measured (iR-free) cell voltages at elevated pressure and 1 bar reference pressure is plotted in Fig. 2c. The corresponding Nernst shifts according to Eq. (2) at 60 °C operating temperature are indicated by horizontal dashed lines. At very small current densities (up to about 0.1 A/cm^2), the experimentally determined voltage changes perfectly match the respective Nernstian shifts for all investigated cathode pressures (3, 5, and 10 bar).

For a cathode pressure of 10 bar, e.g., both the expected and measured voltage shifts are equal to 33 mV. However, the cell voltage increase becomes progressively lower as current density increases, revealing a better-than-expected sub-Nernstian voltage response at higher current densities. Similar observations in other studies have been attributed to improved mass transport at high current densities and pressures as a result of a pressure gradient between the cathode catalyst layer and flow-field channel [39]. The fitted model curves, shown as solid lines in Fig. 2, accurately match the experimental data with a root mean square deviation (RMSD) of only 1.5 mV, cf. Table 1. In particular, the model precisely reproduces the sub-Nernstian voltage response observed in Fig. 2c for currents up to 0.6 A/cm^2. Since the model does not contain any mass-transport terms, this result demonstrates the kinetic origin of the sub-Nernstian pressure effect, which is further analysed in the Discussion section. At higher currents, we observe a very small systematic deviation from experimental voltage differences. A possible explanation for this is a local oversaturation with hydrogen in the cathode catalyst layer at higher current densities as reported in

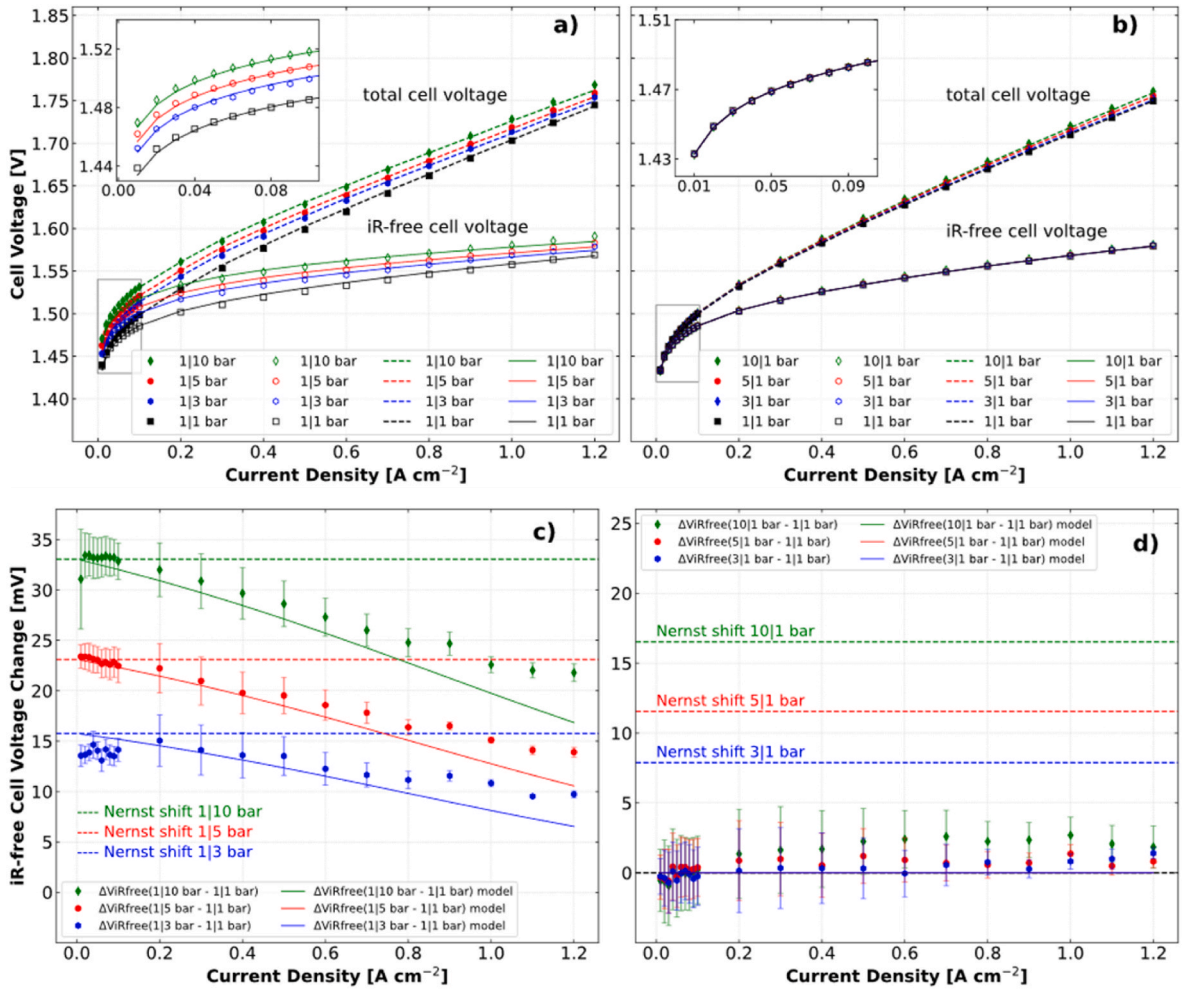


Fig. 2. Results from differential pressurisation mode. a) and b): Total cell voltage (filled markers) and iR-free cell voltage (non-filled markers) as a function of current density obtained from experiments, and the respective fitted model curves (dashed and solid lines). Insets show a magnification of the iR-free cell voltage curves at very low current densities. c) and d): Change in iR-free cell voltage for elevated pressures with reference to 1|1 bar. The corresponding Nernst shifts are indicated by horizontal dashed lines. a) and c): Cathode pressurisation at a constant anode pressure of 1 bar. b) and d): Anode pressurisation at a constant cathode pressure of 1 bar.

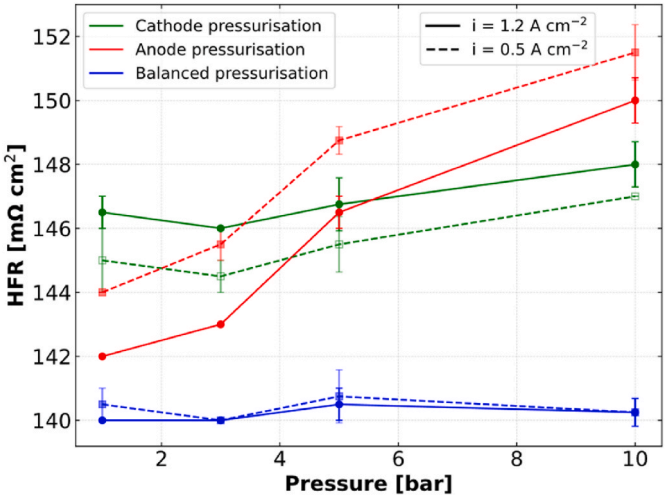


Fig. 3. Dependence of HFR on operating pressure at 0.5 and 1.2 A/cm^2.

Ref. [68] This effect will be considered in future investigations.

Differential mode: anode pressurisation. Fig. 2b shows the total and iR-free cell voltage as a function of current density under different anode (oxygen) pressures and a constant cathode (hydrogen) pressure of 1 bar. In contrast to the results from cathode pressurisation (cf. Fig. 2a), only very small voltage changes due to anode pressure increase are observed at the level of the total cell voltage. Similar behaviour was reported in a study where the anode pressure was varied from 1 to 6 bar at 65 °C [36]. After iR-subtraction, the resulting iR-free cell voltages were unaffected by anode pressure as shown by overlapping curves (Fig. 2b). This shows that the slight shifts observed in the total cell voltage were due to a weak effect of anode pressure on the HFR, with slightly higher HFR values at elevated pressures (Fig. 3). Similar observations were made by Martin et al., [69] who attributed this effect to a possible deformation of the membrane and catalyst layer into the channels of the cathode flow field, resulting in reduced contact area at increased anode pressures. The absence of anode pressure effects on the iR-free cell voltage is reflected by near zero voltage changes, as shown in Fig. 2d. Whereas for cathode pressurisation, the voltage shifts accurately matched the expected Nernst shifts at small current densities (cf. Fig. 2c), the voltage shifts were essentially zero for the case of anode pressurisation. The maximum observed shift by about 3 mV at 1 A/cm^2 and 10 bar anode pressure is still negligible compared to experimental error margins. The fitted model curves, shown as solid lines in Fig. 2, accurately match the experimental data and correctly describe the absence of anode pressure effects on the iR-free cell voltage, which is

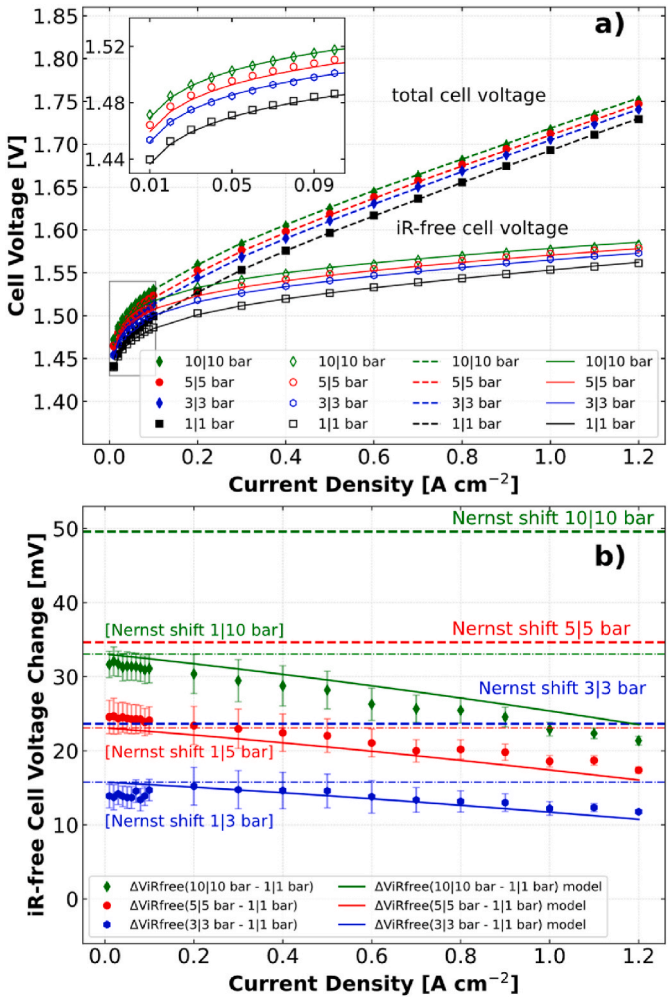


Fig. 4. Results from balanced mode pressurisation. a) Total cell voltage (filled markers) and iR-free cell voltage (non-filled markers) as a function of current density obtained from experiments, and the respective fitted model curves (dashed and solid lines). The inset shows a magnification of the iR-free cell voltage curve at very low current densities. b) Change in iR-free cell voltage for elevated pressures with reference to 1|1 bar. The corresponding total Nernst shifts are indicated by horizontal dashed lines, and horizontal dash-dotted lines indicate the partial Nernst shifts accounting for hydrogen (cathode) pressure changes only.

due to the independence of the OER kinetic branch from oxygen pressure in Eq. (9), while the pressure-dependent ORR branch is negligible at PEMWE operation potentials.

Balanced mode pressurisation. Fig. 4a shows the total and iR-free cell voltage as a function of current density under balanced mode operation. The cell voltage was observed to increase with increasing pressure, similar to the results for cathode pressurisation in differential mode (Fig. 2a). The iR-free cell voltage exhibited the same trend as the total cell voltage when both anode and cathode pressure are increased simultaneously. Balanced pressurisation results in Fig. 3 shows that the influence of operating pressure on HFR is insignificant. Similar results were reported by Suermann et al. [33] for studies conducted at 50 °C and pressures ranging from 1 to 100 bar. The change in iR-free cell voltage compared to 1 bar reference pressure, shown in Fig. 4b, was observed to be lower than predicted by the Nernst equation (horizontal dashed lines in Fig. 4b) and progressively decreased with increasing current density. Also plotted in Fig. 4b is the partial Nernst shift accounting for the hydrogen (cathode) pressure contribution only. The results show that the increase in iR-free cell voltage at current densities lower than 0.1 A/cm^2 was in very good agreement with the partial Nernst shift due to hydrogen pressure (33 mV at 10 bar hydrogen, as compared to 50 mV expected under both 10 bar hydrogen and oxygen). Thus, the iR-free voltage response under balanced pressurisation can be described as the independent superposition of the individual effects of anode and cathode pressurisation as observed in respective differential modes. The fitted model curves, shown as solid lines in Fig. 4, accurately match the experimental data. In particular, the model precisely reproduces the partial Nernst shifts of the cell voltage at low current densities and the decreasing trend of the voltage response with increasing current densities, cf. Fig. 4b.

Tafel analysis. Semi-logarithmic Tafel plots of the iR-free cell voltage vs. current density are shown in Fig. 5 for different pressures in balanced operation mode. Findings from differential operation are shown in Figs S.3 and S.4 of the SI. For all pressures investigated, a linear Tafel behaviour is apparent at low current densities with a fitted Tafel slope (dashed lines in Fig. 5) equal to 46.4 ± 0.4 mV/dec. Deviations from the extrapolated Tafel lines are observed at current densities higher than 0.2 A/cm^2 with an upward bending of the experimental data plots. Remarkably, the fitted curves of the cell voltage model, also shown in Fig. 5, accurately reproduce both the linear Tafel regime at low current densities and the upward bending of the Tafel plots at higher current densities. These findings will be further analysed in the Discussion section.

5. Discussion

The experimental results have demonstrated a sub-Nernstian cell voltage response to increased cathode pressure in both differential operation mode (with constant anode pressure) and balanced pressure mode. It was also found that anode pressurisation in both differential and balanced modes did not have any noticeable effect on the iR-free cell voltage curve. More specifically, under all pressurisation modes, the iR-free cell voltage at very low current densities precisely followed the Nernst equation accounting for the hydrogen pressure only, while ignoring the contribution of the oxygen pressure. With increasing current density, the cell voltage change decreased, clearly falling below the expected minimum Nernstian shift. The sub-Nernstian response of the cell voltage to pressure increase at both the hydrogen and oxygen electrodes is a remarkable experimental observation. Because the Nernstian limit corresponds to the cost of (ideal) isothermal gas compression, the sub-Nernstian voltage increase in pressurised PEMWE operation provides the possibility for electrolyser stack electrical energy savings. Pressurised PEMWE effectively decreases irreversible kinetic energy losses, which are converted into thermodynamically useful gas

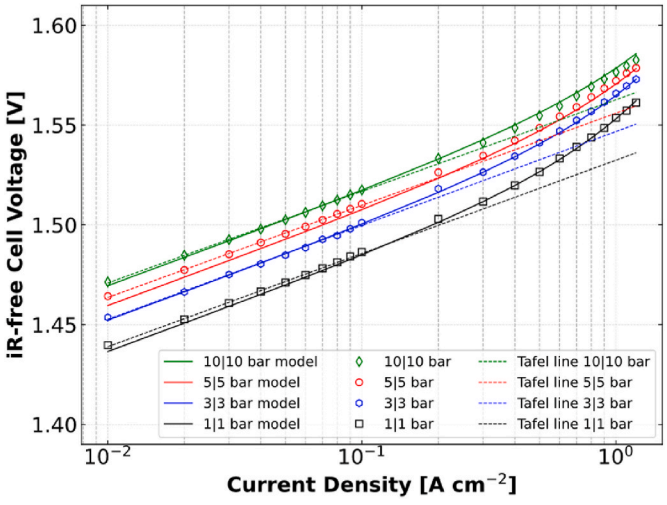


Fig. 5. Tafel plots of the iR-free cell voltages at different pressures in balanced mode incl. fitted Tafel lines (dashed) and full model fits (solid lines).

compression. The fact that the cell voltage approaches the Nernstian shift in the limit of very small current densities demonstrates that this finding is fully consistent with thermodynamic requirements. In other words, energy savings are achieved when comparing two systems under *non-equilibrium* conditions: pressurised PEMWE versus ambient-pressure PEMWE with post-compression, both compared at the same *non-zero* current density. This finding aligns with the broad consensus regarding reduced system energy requirement [17] and economical benefits [70] of high-pressure PEMWE compared to atmospheric PEMWE coupled with mechanical compression.

These experimental findings agree with previously reported observations [4,18,33,40,71]. Müller-Dollinger et al. [4] suggested that the better-than-expected performance under pressurised operation in balanced mode was due to better electrodes compression and increase in local temperature with positive effect on reaction kinetics. In studies conducted in balanced pressure mode by Bernt et al., [71] it was concluded that the expected increase in anode equilibrium potential must have been compensated by some beneficial effect of elevated oxygen pressure on other overvoltage contributions. As for cathode side pressurisation, it was suggested that the sub-Nernstian shift was the result of the reduction a mass transport overpotential due to pressure gradient between the flow-field channel and cathode catalyst layer at high H_2 pressures [71]. Several studies attributed similar experimental observations to mass transport related effects [18,40]. Nouri-Khorasani et al. [41] who modelled oxygen bubbles in the PEMWE porous transport layer (PTL) suggested that a decrease in mass transport overpotential occurs at elevated pressures to counterbalance the pressure-induced Nernstian effect. Suermann et al. [33] suggested that the phenomena observed are related to both kinetic and mass transport effects with kinetic losses being the dominant effect for currents up to 2 A/cm^2. The authors proposed two possible explanations for the kinetics improvements: First, the wetting of the catalyst's micropores resulting in an increase in electrochemically active surface area. Second, an increase in apparent exchange current density as a result of the influence of pressure on the standard Gibbs energy of activation of the rate determining step.

As a main result of the present work, it is demonstrated that the experimentally observed sub-Nernstian pressure effect can be readily explained from basic kinetic considerations, as implemented in the developed cell voltage model. The Butler-Volmer-type kinetic model accurately fitted the experimental data sets in both differential and balanced pressure modes across the entire current density range under investigation (Figs. 2 and 4, respectively), with very small RMSD values between the fitted model curves and experimental data, cf. Table 1. The sensitivity of the cell voltage to individual kinetic parameters is indicated by their standard deviations reported in Table 1. The anode kinetic parameters exhibit standard deviations corresponding to relative standard errors consistently below 10% indicating high sensitivity of cell voltage to anode kinetics. Cathode kinetics parameters on the other hand are associated with relatively larger standard deviations errors indicating lower cell voltage sensitivity to these parameters. Further increasing cathode kinetics is expected to have minimal to no effect on the overall performance. The low RMSD shows that the model captures the essential aspects required to adequately describe and explain the observed sub-Nernstian pressure effects. It is worth highlighting that no mass transport effects must be invoked to explain the measured PEMWE characteristics under pressurised operation in the investigated current density range (up to 1.2 A/cm^2). Although the experiments were deliberately restricted to the kinetically controlled regime in order to isolate intrinsic pressure effects, the kinetic origin of the sub-Nernstian response identified here is not intrinsically limited to low current densities. At higher currents, additional effects such as mass transport and gas crossover may superimpose on the same fundamental kinetic behaviour without redefining its origin.

While the Nernst shift of the voltage at equilibrium is correctly reproduced, the operating cell voltage under non-equilibrium conditions, i.e., for non-zero current densities, is not necessarily affected by the same shift. This is in stark contrast to conventional modelling approaches that employ the (shifting) reversible voltage V_{eq} as a reference for the breakdown of the total cell voltage in terms of overvoltage losses. This choice of V_{eq} as voltage reference is the origin of a misleading expectation that the pressure-induced thermodynamic Nernstian shift would affect the entire polarisation curve as a whole and produce a constant parallel shift to which other overvoltage terms describing activation and mass-transport losses are referenced. The present approach, on the other hand, treats the thermodynamic and activation effects of pressurisation on an equal footing, emphasising their common kinetic origin.

To further analyse the findings, Fig. 6 presents fitted model plots of the anode and cathode overpotential terms, $E_a - E_{a,0}$ and $E_c - E_{c,0}$, defined vs. fixed reference potentials, as a function of the current density according to the model equations (8) and (9) for different pressures in balanced mode. The individual branches of the respective forward and backward reactions are also shown. A significant overpotential of about 0.3 V is observed on the anode side (Fig. 6b), which is due to the sluggishness of the oxygen evolution reaction (OER) [72] and reflected in the very small fitted value of the exchange current density $i_{0,a}$ (cf. Table 1). Therefore, the current associated with the reverse ORR is essentially zero under electrolyser operating conditions. Since the oxygen pressure is only affecting the negligible ORR branch and not the OER, cf. Eq. (9), an increase in pressure does not influence the anode overpotential. The cathode potential (Fig. 6c and d) negatively shifts (increased cathodic overpotential) with increasing cathode (hydrogen) pressure. It should be noted that the current density axis refers to the cell current density, i.e., the negative of the respective kinetic current density, $i = -i_{kin,c}$, cf. Eq. (10). At low current densities (in forward, i.e., HER direction), a significant contribution of the backward HOR branch is observed, which is due to the fast kinetics of the HOR/HER as reflected in the large fitted value of the exchange current density $i_{0,c}$ (cf. Table 1). Accordingly, close to the equilibrium potential (zero current intercept in Fig. 6c), the shape of the potential vs. current curve is determined by the competing rates of the HER and HOR. In this region, the magnitude of activation losses is the result of contributions from *i)* HER, entirely governed by the exchange current density $i_{0,c}$, tied to the nature of the catalyst and *ii)* HOR, dependent on both pressure and exchange current density $i_{0,c}$. Due to its hydrogen-pressure dependence, cf. Eq. (8), the HOR rate becomes enhanced as the pressure increases, shifting the equilibrium potential in negative direction according to the Nernst equation, which is a direct visualisation of the basic concept of a dynamic equilibrium in chemical kinetics. The equilibrium state is thereby characterized by a balance between the forward and backward reaction rates, known as the principle of detailed balance. Consequently, the thermodynamic and kinetic contributions to the pressure-dependence are intertwined. This fundamental perspective is ignored in the common separation into “thermodynamic” (i.e., Nernstian) and “kinetic” contributions to the pressure effect, which has precluded the clear picture revealed by the present modelling approach. As current density increases, the influence of HOR becomes less significant, resulting in a downward bending and a decreased potential difference between the kinetic current curves at different pressures. This is the origin of the sub-Nernstian response of the cell voltage to cathode pressure increase observed in experiments, cf. Figs. 2c and 4b. Since the HER branch is independent of hydrogen pressure, cf. Eq. (8) with $m_{HER} = 0$, the kinetic current curves under different pressures eventually merge at large current densities where the HOR becomes negligible, which is shown in Fig. 6c. At that point, the curves approach the exponential form of the sole HER branch. The kinetic model thus predicts that the cell voltage becomes essentially independent of the operating pressure at large current densities, at least when other, possibly pressure-dependent factors such as mass-transport losses are ignored. These considerations show that increasing the PEMWE operation pressure, either at the anode

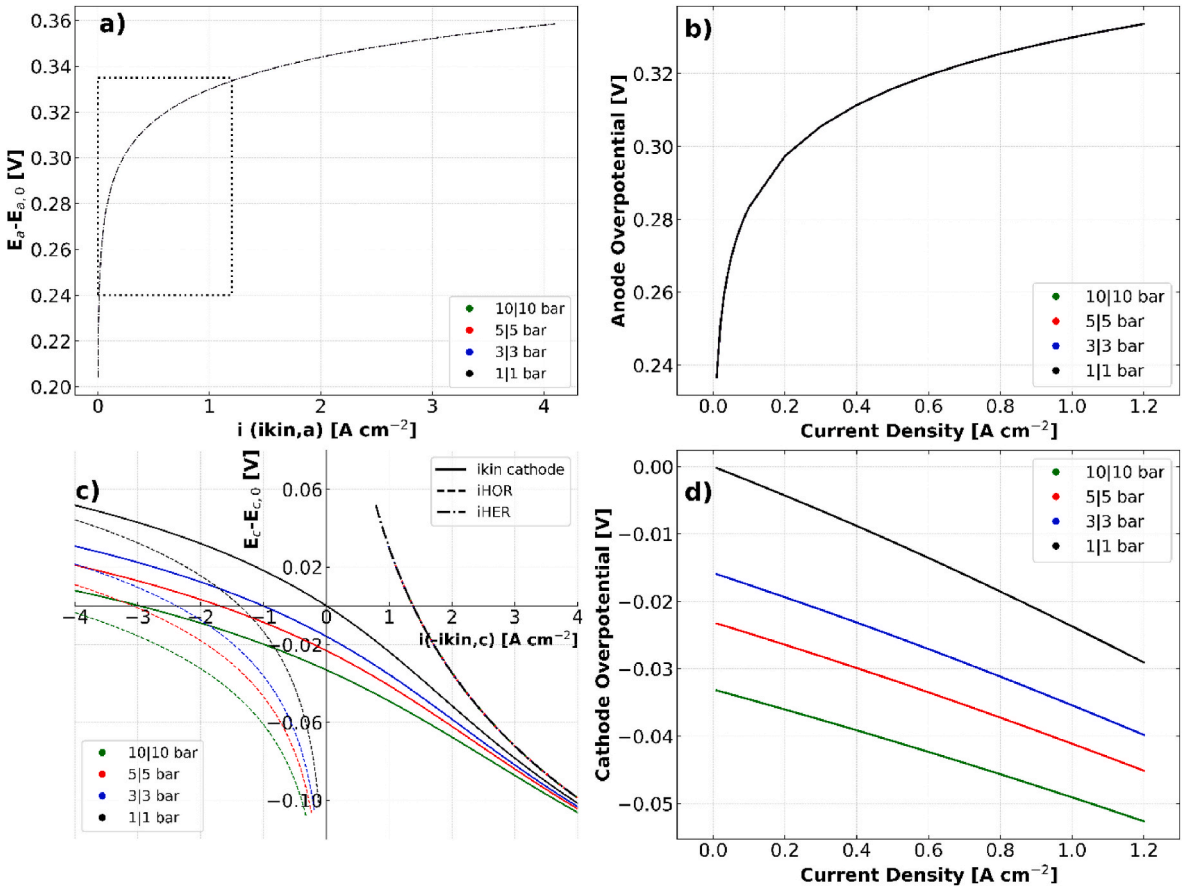


Fig. 6. Fitted model plots for balanced pressurisation. Anode (a) and cathode (c) overpotentials, $E_a - E_{a,0}$ and $E_c - E_{c,0}$, defined vs. the respective fixed reference potentials (cf. model equations (8) and (9)), as a function of kinetic current density for different (balanced) pressures in an extended current density range. The individual branches of the respective forward (HER) and backward (HOR) reactions at the cathode are also shown. Only the forward branch (OER) of the anode reaction is shown since ORR has no effect on the overall reaction under PEMWE operating conditions. (b) and (d): Plots of the anode and cathode potential in the experimental current density range (0 – 1.2 A/cm^2), as indicated by dashed rectangles in (a) and (c).

and/or cathode, effectively converts part of the irreversible kinetic losses into useful gas-compression energy [42].

The values of the fitted model parameters for the different pressurisation modes agreed to within reasonable margins, cf. Table 1. The anode exchange current density was about seven orders of magnitude smaller than the cathode exchange current density, as expected for the sluggish OER vs. fast HER kinetics [73]. It should be noted that the values of the exchange current densities reported in cf. Table 1 were normalised with respect to the geometric area of the cell, while for direct comparison with other studies normalisation by the electrochemical surface area (ECSA) of the catalysts is required, which was not possible to be determined in the present study. It is however observed that the values of the anode exchange current density fall within the same order of magnitude as those reported in other studies for both PEMWE and RDE experiments [18,73,74]. Likewise, the values of the cathode exchange current density lie within an order of magnitude of other reported values [46,75]. An OER transfer coefficient of about $\alpha_{OER} = 1.4 \pm 0.1$ was obtained from the fits for different pressurisation modes. This value corresponds to a Tafel slope of 47 mV/dec at 60 °C, which falls within the range of values reported in the literature [33,40,76]. The fitted value of the HER transfer coefficient was about $\alpha_{HER} = 0.35 \pm 0.05$ (Tafel slope of about 190 mV/dec) across the different pressurisation modes, with a corresponding value of $\alpha_{HOR} = 1 - \alpha_{HER} = 0.65 \pm 0.05$ for the HOR transfer coefficient (Tafel slope of about 100 mV/dec). These values are slightly more asymmetric in comparison to other reported values of about 0.5 for both transfer coefficients [46,75,77,78].

The Tafel analysis of the iR-free cell voltage has shown the commonly observed linear behaviour in the low current density region for all pressures (Fig. 5). The Tafel slope value in the linear region (46.4 ± 0.4 mV/dec) is in good agreement with the value of 47 mV/dec corresponding to the fitted OER transfer coefficient ($\alpha_{OER} = 1.4$). Moreover, the Tafel slope was found to be unaffected by pressure, in agreement with results reported by Suermann et al. [33] With increasing current densities, a deviation from the extrapolated Tafel line was observed. Similar reported observations were sometimes associated with the existence of more than one Tafel line [79,80] and ascribed to mass transport losses on the anode side of the electrolyser [81–85]. Other studies excluded limitations in mass transport as the origin of Tafel line deviations at increased current densities, which were rather ascribed to a change in the OER reaction mechanism [80,86]. The present results show that neither mass-transport effects nor changes in reaction mechanism must be invoked to explain the observed deviations from the extrapolated Tafel lines. The upward bending of the experimental Tafel plots is accurately described by the cell voltage model, as shown in Fig. 5. The effect can thus be explained from the basic kinetic model equations (8) and (9) with single exponential branches (corresponding to single Tafel slopes) for each of the considered reactions of HER/HOR and OER/ORR. For deeper analysis, Fig. 7 presents (semi-logarithmic) Tafel plots of the deconvoluted anode (OER/ORR) and cathode (HER/-HOR) contributions of the model fitted for balanced pressure mode. Anode kinetics (Fig. 7a) are solely determined by the OER as represented by a straight Tafel line, which is responsible for the linear Tafel behaviour of the combined anode and cathode kinetics at low current densities, shown in Fig. 7c. The cathode kinetics (Fig. 7b) present an

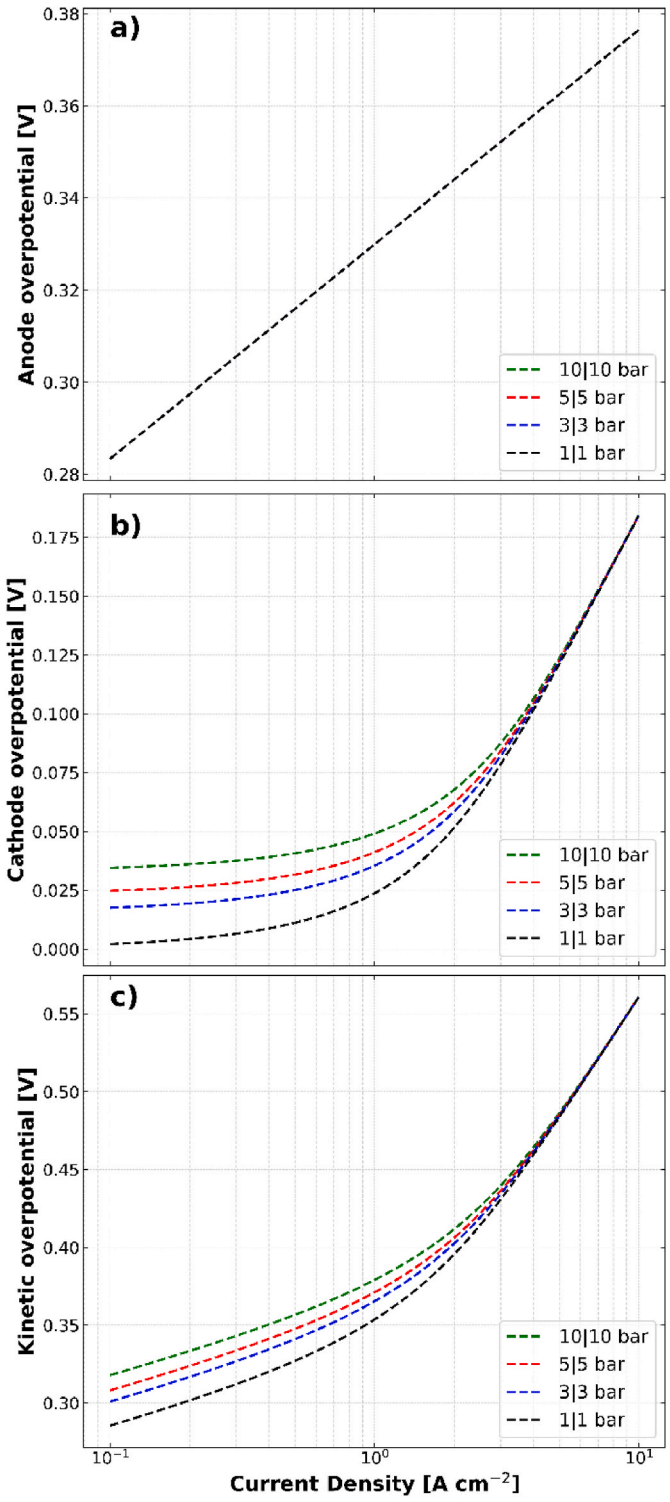


Fig. 7. Tafel plots of the kinetic model for (a) anode (OER/ORR, Eq. (9)), (b) cathode (HER/HOR, Eq. (8)), and (c) the combined contributions, using the model parameters fitted for balanced-mode pressurisation.

almost horizontal Tafel plot at low current densities, which results from the overlap of the competing HER and HOR branches. With increasing current densities, the contribution of the HOR branch becomes suppressed, and the HER/HOR Tafel plot bends upward to converge to the sole HER branch with a Tafel slope of about 190 mV/dec according to the fitted transfer coefficient of about $\alpha_{\mathrm{HER}} = 0.35$, as discussed above. This upward bending of the cathode Tafel plot due to the vanishing influence of the HOR backward reaction explains the experimentally observed deviation from the extrapolated Tafel line in the iR-free cell voltage (Fig. 5). While conventional voltage breakdown may attribute the upward bending to mass transport limitations, our findings support a kinetic origin. Polarisation curves within the entire current density range and across multiple pressures were accurately reproduced without the need to invoke mass-transport related terms.

As shown in Fig. 7c, extrapolating the model curves to larger current densities, the upward bending is seen to represent the transition from the low-current-density linear Tafel region (with the sole OER slope) to a second high-current-density linear Tafel region with a slope equal to the sum of the OER and HER Tafel slopes (237 mV/dec according to the fitted model parameters). Tafel plots of the deconvoluted anode and cathode overpotential contributions of the model fitted for differential pressure mode are shown in Fig S.5 SI. In several studies, the voltage losses due to cathode reaction kinetics were assumed to be insignificant [27,39,83]. The present analysis, on the contrary, demonstrates that the cathode kinetics have a significant impact on the experimentally observed characteristics of the cell voltage, producing two linear regions in the Tafel plot. These findings are supported by a recent study where the nonlinear frequency response method has been used to analyse electrolyser performance [87]. Results from this study have also shown that the contributions of cathode kinetics to the total cell overvoltage become pronounced at high current densities.

6. Conclusion

In this combined experimental–theoretical study, the effect of differential cathode, differential anode, and balanced pressurisation on the performance of a proton exchange membrane water electrolyser was investigated, employing “mild” pressure variations up to 10 bar. Experiments have shown a sub-Nernstian response of the total cell voltage to pressure increase in both differential and balanced pressure operation modes. At very low current densities, voltage changes in agreement with the partial Nernst shift due to the cathode (hydrogen) pressure were found. The observed voltage changes decreased with increasing current densities. Anode (oxygen) pressure did not have any noticeable effect on iR-free cell voltages in the investigated current range up to 1.2 A/cm^2. The established sub-Nernstian voltage response indicates that high-pressure PEMWE can effectively offset some of the voltage cost of in-situ gas compression. This experimental evidence supports the broader literature consensus that high-pressure PEMWE offers a net energy advantage and economic benefit over atmospheric systems requiring downstream mechanical compression. A novel cell voltage model was shown to accurately fit the experimental data and explain the observed pressure effects, where kinetic rate expressions for the hydrogen and oxygen electrode reactions accounted for both the forward and backward directions and were formulated using a fixed potential reference. The studies revealed the kinetic origin of the sub-Nernstian shift, demonstrating that higher pressure operation effectively converts part of the irreversible activation losses into useful gas compression energy. A deconvolution of the total cell voltage based on the model further showed that the contribution of the cathode overpotential becomes significant at higher current densities, explaining the emergence of a second linear region in the Tafel plot of the iR-free cell voltage. The kinetic model for the cell voltage thus provided simple and intuitive explanations for several intriguing phenomena in (pressurised) PEMWE, which so far had been ascribed primarily to mass transport losses. This insight is expected to give direction to future developments in PEMWE analysis and modelling. While this study validates the pressure-dependent kinetic studies for a specific cell configuration within a limited current and pressure range, the governing equations are derived from fundamental electrochemical theory and are expected to be adaptable to different configurations. The kinetic origin of the sub-Nernstian shift reported in the present study will be fundamental in deconvoluting effects due to more complex phenomena expected at

higher current densities. The effect of elevated pressures at higher current densities will be considered in subsequent works. Further studies should also include detailed microkinetics model formulations.

CRediT authorship contribution statement

Katende Jonathan Kabamba: Writing – review & editing, Writing – original draft, Visualization, Validation, Software, Methodology, Investigation, Formal analysis, Data curation, Conceptualization. **Tobias Binninger:** Writing – review & editing, Validation, Supervision, Software, Methodology, Investigation, Formal analysis, Conceptualization. **Boris Bensmann:** Writing – review & editing, Validation, Formal analysis, Conceptualization. **Rhiyaad Mohamed:** Writing – review & editing, Supervision, Resources, Project administration, Methodology, Funding acquisition, Formal analysis, Conceptualization.

Declaration of competing interest

The authors declare that they have no known competing financial interests or personal relationships that could have appeared to influence the work reported in this paper.

Acknowledgements

The authors acknowledge financial support from the South African Department of Science and Innovation (DSTI) through the HySA/Catalysis Centre of Competence programme. T.B. contributed to this work within the framework of the Helmholtz Association's programme *Materials and Technologies for the Energy Transition*, under the topic *Chemical Energy Carriers* and the subtopic *Electrochemistry for Hydrogen*. The authors gratefully acknowledge the Institute of Electric Power Systems (IFES) , where all experimental measurements reported in this study were conducted. The authors also thank Prof. Dr.-Ing. Richard Hanke-Rauschenbach, head of the Electric Energy Storage Systems section at IFES, for his support.

Appendix A. Supplementary data

Supplementary data to this article can be found online at https://doi.org/10.1016/j.ijhydene.2026.154454.

References

[1] Squadrito G, Maggio G, Nicita A. Renew Energy 2023;216:119041.
[2] Sharaf OZ, Orhan MF. Renew Sustain Energy Rev 2014;32:810–53.
[3] Gahleitner G. Int J Hydrogen Energy 2013;38:2039–61.
[4] Müller-Dollinger A, Bittner R, Czarnetzki W, Kallo J. Int J Hydrogen Energy 2023;48:31078–90.
[5] Yang X, Nielsen CP, Song S, Mcelroy MB. Nat Energy 2022;7:955–65.
[6] Rissman J, Bataille C, Masanet E, Aden N, Morrow WR, Zhou N, Elliott N, Dell R, Heeren N, Huckestein B, Cresko J, Miller SA, Roy J, Fennell P, Cremmins B, Koch Blank T, Hone D, Williams ED, de la Rue du Can S, Helseth J. Appl Energy 2020;266:114848.
[7] Carmo M, Fritz DL, Mergel J, Stolten D. Int J Hydrogen Energy 2013;38:4901–34.
[8] Bauer C, Desai H, Heck T, Sacchi R, Schneider S, Terlouw T, Treyer K, Zhang X. Electricity storage and hydrogen technologies, costs and impacts on climate change. Paul Scherrer Institute; 2022.
[9] Van Der Spek M, Banet C, Bauer C, Gabrielli P, Goldthorpe W, Mazzotti M, Munkejord ST, Røkke NA, Shah N, Sunny N, Sutter D, Trusler JM, Gazzani M. Energy Environ Sci 2022;15:1034–77.
[10] Zakeri B, Syri S. Renew Sustain Energy Rev 2015;42:569–96.
[11] Marshall A, Børresen B, Hagen G, Tsypkin M, Tunold R. Energy 2007;32:431–6.
[12] Millet P, Ngameni R, Grigoriev SA, Mbemba N, Brisset F, Ranjbari A, Etiévant C. Int J Hydrogen Energy 2010;35:5043–52.
[13] Maric R, Yu H. Proton exchange membrane water electrolysis as a promising technology for hydrogen production and energy storage. 2019.
[14] Suermann M, Pătru A, Schmidt TJ, Büchi FN. Int J Hydrogen Energy 2017;42:12076–86.
[15] Jones DSJ. Handbook of petroleum processing, 1. Springer International Publishing; 2015. p. 125–98. ch. [Chapter 3].
[16] Cheema II, Krewer U. RSC Adv 2018;8:34926–36.
[17] Salehmin MNI, Husaini T, Goh J, Sulong AB. Energy Convers Manag 2022;268.115985-115985.
[18] Grigor'ev SA, Khaliullin MM, Kuleshov NV, Fateev VN. Russ J Electrochem 2001;37:819–22.
[19] Hancke R, Holm T, Ulleberg Ø. Energy Convers Manag 2022;261. 115642-115642.
[20] Bensmann B, Hanke-Rauschenbach R, Müller-Syring G, Henel M, Sundmacher K. Appl Energy 2016;167:107–24.
[21] Marangio F, Santarelli M, Cali M. Int J Hydrogen Energy 2009;34:1143–58.
[22] Sartory M, Wallnöfer-Ogris E, Salman P, Fellinger T, Justl M, Trattner A, Klell M. Int J Hydrogen Energy 2017;42:30493–508.
[23] Dang J, Zhang J, Deng X, Yang S, Liu B, Zhu X, Li Y, Yang F, Ouyang M. J Power Sources 2023;563:232776.
[24] Hancke R, Bujlo P, Holm T, Ulleberg Ø. J Power Sources 2024;601:234271.
[25] Ishikawa H, Haryu E, Kawasaki N, Daimon H. Honda R&D tech Rev 2016;28:9.
[26] Olivier P, Bourasseau C, Bouamama PB. Renew Sustain Energy Rev 2017;78:280–300.
[27] García-Valverde R, Espinosa N, Urbina A. Int J Hydrogen Energy 2012;37:1927–38.
[28] Bessarabov D, Wang H, Li H, Zhao N. PEM electrolysis for hydrogen production. Boca Raton: CRC Press; 2015.
[29] Yigit T, Selamet OF. Int J Hydrogen Energy 2016;41:13901–14.
[30] Zhao H, Du H, Zhang T, Wang H. Energy Convers Manag 2022;268:116019.
[31] Han B, Steen M, Mo JK, Zhang FY. Int J Hydrogen Energy 2015;40:7006–16.
[32] Tijani AS, Afiqah N, Kamarudin B, Athirah F, Mazlan B, Binti Kamarudin NA, Binti Mazlan FA. Int J Hydrogen Energy 2018;43:9119–32.
[33] Suermann M, Schmidt TJ, Büchi FN. Electrochim Acta 2016;211:989–97.
[34] Selamet ÖF, Acar MC, Mat MD, Kaplan Y. Int J Energy Res 2013;37:457–67.
[35] Correa G, Marocco P, Muñoz P, Falagüerra T, Ferrero D, Santarelli M. Int J Hydrogen Energy 2022;47:4315–27.
[36] Garcia-Navarro JC, Schulze M, Friedrich KA. J Power Sources 2019;431:189–204.
[37] Grigoriev SA, Porembskiy VI, Korobtsev SV, Fateev VN, Auprêtre F, Millet P. Int J Hydrogen Energy 2011;36:2721–8.
[38] Ojong ET, Kwan JTH, Nouri-Khorasani A, Bonakdarpour A, Wilkinson DP, Smolinka T. Int J Hydrogen Energy 2017;42:25831–47.
[39] Bernt M, Gasteiger HA. J Electrochem Soc 2016;163:F3179–89.
[40] Bernt M, Siebel A, Gasteiger HA. J Electrochem Soc 2018;165:F305–14.
[41] Nouri-Khorasani A, Tabu Ojong E, Smolinka T, Wilkinson DP. Int J Hydrogen Energy 2017;42:28665–80.
[42] Binninger T, Heinritz A, Mohamed R. J Chem Phys 2023;158:124129.
[43] Bratsch SG. J Phys Chem Ref Data 1989;18:1–21.
[44] Heinritz A, Binninger T, Herranz J, Rodriguez P, Schmidt TJ. J Electrochem Soc 2024;171:114511.
[45] Prats H, Chan K. Phys Chem Chem Phys 2021;23:27150–8.
[46] Kucernak AR, Zalitis C. J Phys Chem 2016;120:10721–45.
[47] Sheng W, Zhuang Z, Gao M, Zheng J, Chen JG, Yan Y. Nat Commun 2015;6:5848.
[48] Strmcnik D, Uchimura M, Wang C, Subbaraman R, Danilovic N, van der Vliet D, Paulikas AP, Stamenkovic VR, Markovic NM. Nat Chem 2013;5:300–6.
[49] Tang MT, Liu X, Ji Y, Norskov JK, Chan K. J Phys Chem C 2020;124:28083–92.
[50] Razzaq S, Exner KS. iScience 2024;27:108848.
[51] Garcia AC, Koper MTM. ACS Catal 2018;8:9359–63.
[52] Newman J, Thomas-Alyea KE. Electrochemical systems. John Wiley & Sons, Inc.; 2004.
[53] Miličić T, Altaf H, Vorhauer-Huget N, Živković LA, Tsotsas E, Vidaković-Koch T. Processes 2022;10:2417.
[54] Espinosa-López M, Darras C, Poggi P, Glises R, Baucour P, Rakotondrainibe A, Besse S, Serre-Combe P. Renew Energy 2018;119:160–73.
[55] Dale NV, Mann MD, Salehfar H. J Power Sources 2008;185:1348–53.
[56] Görgün H. Int J Hydrogen Energy 2006;31:29–38.
[57] Shin H, Kim K, Jang D, shin H, Lim CH, Kim K-H, Kang S. Appl Therm Eng 2025;279:127676.
[58] Keller R, Rauls E, Hehemann M, Müller M, Carmo M. Control Eng Pract 2022;120:104992.
[59] Biaku CY, Dale NV, Mann MD, Salehfar H, Peters AJ, Han T. Int J Hydrogen Energy 2008;33:4247–54.
[60] Hamdan M. PEM electrolyzer incorporating an advanced low-cost membrane, giner, inc./giner electrochemical systems. Newton, MA: LLC; 2013.
[61] Hensle N, Horstmann de la Viña J, Winterholler N, Hoffmann J, Armbruster S, Lindner A, Weber A, Smolinka T. ACS Appl Energy Mater 2025;8:7107–24.
[62] Hensle N, Lickert T, Winterholler N, Smolinka T, Weber A. J Power Sources 2025;654:237865.
[63] Pasmay FN, Litster S. J Power Sources 2025;633:236452.
[64] Gawas R, Kushner DI, Peng X, Mukundan R. Energy Environ Sci 2025;18:4625–31.
[65] Papakonstantinou G, Sundmacher K. Electrochem Commun 2019;108.
[66] Falcão DS, Pinto AMFR. J Clean Prod 2020;261:121184.
[67] Wei C, Sun S, Mandler D, Wang X, Qiao SZ, Xu ZJ. Chem Soc Rev 2019;48:2518–34.
[68] Trinke P, Keeley GP, Carmo M, Bensmann B, Hanke-Rauschenbach R. J Electrochem Soc 2019;166:F465–71.
[69] Martin A, Trinke P, Stähler M, Stähler A, Scheepers F, Bensmann B, Carmo M, Lehnert W, Hanke-Rauschenbach R. J Electrochem Soc 2022;169.
[70] Benmehel A, Chabab S, Do Nascimento Rocha AL, Chepy M, Kousksou T. Energy Convers Manag X 2024;24:100738.
[71] Bernt MP. PhD, technischen universität münchen. 2019.
[72] Fabbri E, Habereder A, Waltar K, Kötz R, Schmidt TJ. Catal Sci Technol 2014;4:3800–21.
[73] Schuler T, Kimura T, Schmidt TJ, Büchi FN. Energy Environ Sci 2020;13:2153–66.
[74] Kroschel M, Bonakdarpour A, Kwan JTH, Strasser P, Wilkinson DP. Electrochim Acta 2019;317:722–36.

[75] Durst J, Siebel A, Simon C, Hasché F, Herranz J, Gasteiger HA. Energy Environ Sci 2014;7:2255–60.
[76] Bühre LV, McLeod AJ, Trinke P, Bensmann B, Benecke M, Herrera OE, Mérida W, Hanke-Rauschenbach R. J Electrochem Soc 2023;170:094507.
[77] Sheng W, Gasteiger HA, Shao-Horn Y. J Electrochem Soc 2010;157. B1529-B1529.
[78] Choudhury D, Das R, Tripathi AK, Priyadarshani D, Neergat M. Langmuir 2022;38:4341–50.
[79] Papakonstantinou G, Algara-Siller G, Teschner D, Vidaković-Koch T, Schlögl R, Sundmacher K. Appl Energy 2020;280:115911.
[80] Nong HN, Falling LJ, Bergmann A, Klingenhof M, Tran HP, Spöri C, Mom R, Timoshenko J, Zichittella G, Knop-Gericke A, Piccinin S, Pérez-Ramírez J, Cuenya BR, Schlögl R, Strasser P, Teschner D, Jones TE. Nature 2020;587:408–13.
[81] Lee JK, Lee C, Fahy KF, Zhao B, LaManna JM, Baltic E, Jacobson DL, Hussey DS, Bazylak A. Cell Rep Phys Sci 2020;1:100147.
[82] Schuler T, Schmidt TJ, Büchi FN. J Electrochem Soc 2019;166:F555.
[83] Peng X, Satjaritanun P, Taie Z, Wiles L, Keane A, Capuano C, Zenyuk IV, Danilovic N. Adv Sci 2021;8:2102950.
[84] Suermann M, Takanohashi K, Lamibrac A, Schmidt TJ, Büchi FN. J Electrochem Soc 2017;164:F973.
[85] Schuler T, Ciccone JM, Krentscher B, Marone F, Peter C, Schmidt TJ, Büchi FN. Adv Energy Mater 2020;10:1903216.
[86] Frensch SH, Olesen AC, Araya SS, Kær SK. Electrochim Acta 2018;263:228–36.
[87] Milićić T, Muthunayakage K, Vũ TH, Ritschel TK, Živković LA, Vidaković-Koch T. Chem Eng J 2024;496:153889.